Rheol Acta (2007) 46:1197–1209
DOI 10.1007/s00397-007-0208-5

ORIGINAL CONTRIBUTION

Recoverable deformation and morphology after uniaxial elongation of a polystyrene/linear low density polyethylene blend

Ulrich A. Handge · Kenzo Okamoto · Helmut Münstedt

Received: 22 July 2006 / Accepted: 4 May 2007 / Published online: 18 June 2007

Abstract The transient recoverable deformation ratio after melt elongation at various elongational rates and maximum elongations was investigated for pure polystyrene and for a 85 wt.% polystyrene/15 wt.% linear low density polyethylene (PS/LLDPE 85:15) blend at a temperature of 170 °C. The ratio p of the zero shear rate viscosity of LLDPE to that of PS is $p = 0.059 \approx 1:17$. Retraction of the elongated LLDPE droplets back to spheres and end-pinching is observed during recovery. A simple additive rule is applied in order to extract the contribution of the recovery of the elongated droplets from the total recovery of the blend. In that way, the recoverable portion of the PS/LLDPE blend induced by the interfacial tension is determined and compared with the results of a theory based on an effective medium approximation. The effective medium approximation reproduces well the time scale of the experimental data. In addition, the trends that the recoverable deformation increases with elongational rate and maximum elongation are captured by the theoretical approach.

U. A. Handge (✉)
Department of Materials, ETH Zurich, Institute of Polymers, HCI H 529, Wolfgang-Pauli-Strasse 10, 8093 Zurich, Switzerland
e-mail: ulrich.handge@mat.ethz.ch

K. Okamoto · H. Münstedt
Department of Materials Science, Institute of Polymer Materials, Friedrich-Alexander-University Erlangen-Nürnberg, Martensstraße 7, 91058 Erlangen, Germany

Keywords PS/LLDPE blend · Recoverable strain after uniaxial elongation · Morphology development during recovery · Effective medium approximation

Introduction

The increasing technological use of polymer blends has entailed a large interest in understanding the flow properties of multiphase polymer systems. Consequently, the rheological properties of melts of two-phase polymer blends are currently the focus of many theoretical and experimental studies. In these works, the interplay between the morphology and the flow properties of polymer blends is investigated in shear and elongational flows. A key parameter is the interfacial tension between the two polymers which contributes to the viscoelasticity of the blend. The linear viscoelastic properties of blends of two immiscible polymers are generally well described by the model of Palierne (1990) which is widely applied in order to predict the storage and the loss modulus of these polymer blends (Graebling et al. 1993; Vinckier et al. 1996; Minale et al. 1997; Okamoto et al. 1997, 1999b; Jacobs et al. 1999; Fahrländer and Friedrich 1999). In the nonlinear regime, experimental investigations of continuous shear flow (Takahashi et al. 1994a,b; Takahashi and Noda 1995; Vinckier et al. 1997), step shear strain experiments (Okamoto et al. 1999a; Iza and Bousmina 2000) and recovery experiments in shear (Thornton et al. 1980; Gronski et al. 1996) were reported. The theoretical models of Doi and Ohta (1991), Wagner et al. (1999), Almusallam et al. (2000) and Wetzel and

Tucker (2001) partially describe the results of the continuous shear and the step shear strain experiments (Takahashi et al. 1994a,b; Vinckier et al. 1997; Okamoto et al. 1999a). On the other hand, only a few studies explored rheological properties of polymer blends in elongation. Therefore, theoretical and experimental investigations on the elongation of blends of immiscible polymers in the molten state are presently undertaken in order to elucidate the behavior of polymer blends during this basic mode of deformation (Levitt et al. 1997; Mechbal and Bousmina 2004; Heindl 2005; Handge and Pötschke 2004; Handge 2005; Oosterlink et al. 2005; Filipe et al. 2006).

In this article, the focus lies on the influence of the interfacial tension on the recovery of a blend of the two immiscible polymers PS and LLDPE after elongation in the molten state. Recovery experiments of a blend of two immiscible polymers after shear creep and elongation were performed by Gramespacher and Meissner (1995, 1997). The blend components were PS and poly(methyl methacrylate) (PMMA), and the maximum weight fraction of the minor phase was 20 wt.%. Handge and Pötschke (2004) investigated the transient recovery of PS/PMMA blends with much larger weight fractions and with a co-continuous structure and a droplet morphology, respectively. The ratio p of the zero shear rate viscosities of PMMA to PS at measuring temperature was $p = 0.55$ and thus not far away from unity.

A theoretical approach to model the recovery of two-phase polymer blends is described by Handge (2003). In this model, an effective medium approximation is applied with effective values of the Hencky strain rates of the disperse and the matrix phase. In addition, it is assumed that the disperse and the matrix phase are Newtonian fluids. The model agrees well with experimental data for PS/PMMA blends with a viscosity ratio not far from unity (Handge 2003; Handge and Pötschke 2004). Until now, this has been the only comparison between the theory based on the effective medium approximation and experimental data. If the viscosity of the drop phase is much smaller than the viscosity of the matrix phase, additional effects can occur. For example, the drops which were deformed into a filament-like shape with a high surface area can possibly break up during recovery.

In this study, the transient recovery after elongation of a polystyrene/linear low density polyethylene (PS/LLDPE) blend with an initial droplet morphology in the molten state is reported. The weight fraction of the LLDPE in the blend was 15 wt.%. The recoverable portion induced by the interfacial tension was extracted from the total recovery of the blend and compared with the results of the effective medium approximation. In the present work, the time-dependence of recovery after deformation at various elongational rates and maximum elongations and the morphology development of a PS/LLDPE blend is investigated. In comparison to the studies of Gramespacher and Meissner (1997) and Handge and Pötschke (2004) on PS/PMMA blends, another blend component was used resulting in a ratio of the zero shear rate viscosities of $p = 0.059 \approx 1:17$, i.e. much smaller than that of the PS/PMMA system.

Experiments

Materials

The components of the blend are the polystyrene PS 158K (BASF, Germany) and the linear low density polyethylene Escorene LLN 1001 XV (Exxon Chemical, USA). The glass transition temperatures T_g, the melting temperatures T_m, the number averages of the molecular weight M_n, the weight averages of the molecular weight M_w and the zero shear rate viscosities η_0 at a temperature of $T = 170$ °C of these polymers are summarized in Table 1. The interfacial tension Γ between PS and LLDPE at $T = 170$ °C was determined as $5.0\,\mathrm{mNm^{-1}}$ by measuring the surface tension of the components and by the harmonic-mean equation (Heindl et al. 2004; Wu 1982). The blend was prepared by a twin screw extruder at around $T = 200$ °C. The composition ratio of PS/LLDPE was 85:15 by weight which corresponds to 83:17 by volume. Other characteristics of the components and details of the preparation procedure of the blend are reported by Heindl et al. (2004) and Heindl (2005).

Dynamic mechanical measurements

The storage and the loss modulus G' and G'' of the blend components and the blend as a function of the angular frequency ω were determined using a rotational rheometer (Gemini, TA Instruments, USA) with a parallel-plates geometry at $T = 170$ °C. The diameter of the plates was 25 mm, and the gap was set to 1.55 mm.

Table 1 Characteristics of the blend components

	T_g (°C)	T_m (°C)	M_n (g/mol)	M_w (g/mol)	η_0 at 170 °C (Pa s)
PS	95	-	200,000	330,000	230,000
LLDPE	≈ –110	120	62,000	150,000	13,600

A nitrogen gas atmosphere was used during the measurements to minimize the degradation of the sample. The strain amplitude was chosen as 0.003 for the pure PS and the blend, and as 0.06 for the pure LLDPE. The angular frequency ω was varied between $10^{-2}\,s^{-1}$ and $10^{2}\,s^{-1}$.

Uniaxial elongation and recovery

Uniaxial elongation and recovery experiments were carried out with the Münstedt-type extensional rheometer (Münstedt 1979; Münstedt et al. 1998) at $T = 170$ °C. The diameter and the length of the samples ranged between 4.5 and 6 mm and between 25 and 27 mm, respectively. The samples were elongated at different constant Hencky strain rates $\dot{\epsilon}$ to various maximum stretch ratios λ_{max}. The Hencky strain rates were chosen as 0.01 s^{-1}, 0.1 s^{-1} and 0.5 s^{-1} and the maximum stretch ratios of elongation λ_{max} were 4.0, 7.4 and 12.0 which correspond to the maximum Hencky strains $\epsilon_{max} = \ln(\lambda_{max})$ of 1.4, 2.0 and 2.5.

After elongation, the recovery measurements were performed as follows: At the end of elongation at the time $t = t_{max} = \epsilon_{max}/\dot{\epsilon}$, the span length of the sample is very rapidly decreased by an amount ΔL which results in a bending of the sample and in setting the tensile stress to zero at the same time. Due to recovery, the sample length decreases. The time $\Delta t'$ until the sample has attained its straight geometry again is taken as the time needed for the recovery of the sample by ΔL. Repeating this procedure m times, the dependence of the sample length $L(t')$ on the recovery time $t' = t - t_{max}$ is determined by

$$L(t') = L_{max} - \sum_{k=1}^{m} \Delta L_k \tag{1}$$

with

$$t' = \sum_{k=1}^{m} \Delta t'_k. \tag{2}$$

In our series of experiments typical values were $1 \le m \le 60$, $0\ \text{cm} \le \Delta L_k \le 16\ \text{cm}$, and $0.7\ \text{s} \le \Delta t_k \le 700\ \text{s}$. In Eq. 1 the sample length at the beginning of the recovery experiment is denoted by L_{max}. The transient recovered stretch ratio $\lambda_r(t')$ follows from

$$\lambda_r(t') = L_{max}/L(t'). \tag{3}$$

Characterization of morphology

The morphology of the PS/LLDPE 85:15 blend was observed (1) before elongation, (2) at the maximum stretch ratio $\lambda_{max} = 7.4$ for all the strain rates applied and (3) during recovery after elongation at $\dot{\epsilon} = 0.1\ s^{-1}$ up to $\lambda_{max} = 7.4$ and $\lambda_{max} = 12.0$. The elongated samples were quenched at the maximum strain and during recovery at recovery times $t' = 60, 120, 240$ and 480 s. After quenching, the samples were fractured in liquid nitrogen. The quenching time roughly was 5 s which is much smaller than the interfacial relaxation time $\tau_{int} \approx 62$ s. In the initial stage, the stretched polymer chains recoil much faster than the extended drops. The fractured surfaces were analyzed by a scanning electron microscope (SEM, LEO 435VP, Carl Zeiss, Germany). In order to determine the droplet radius before elongation, the radii r_i of the N spherical segments (holes) due to the droplets on the fractured surfaces were determined. The radius r_i corresponds to the radius of a cross section of the ith droplet. Goldsmith (1967) analytically calculated the relation between the visible particle size distribution in a thin slice and the distribution of the true droplet radius. In our case, the fractured surface roughly corresponds to a slice of zero thickness. Then the number average $\langle R_n \rangle$ and the volume average $\langle R_v \rangle$ of the true droplet radius distribution can be estimated by (Goldsmith 1967)

$$\langle R_n \rangle = 4\langle r_n \rangle/\pi \tag{4}$$

$$\langle R_v \rangle = 32\langle r_s \rangle/(9\pi), \tag{5}$$

where $\langle r_n \rangle = (1/N)\sum_{i=1}^{N} r_i$ denotes the measured number average and $\langle r_s \rangle = \sum_{i=1}^{N} r_i^3 / \sum_{i=1}^{N} r_i^2$ the measured area average of the droplet radius. Equation 4 assumes a monodisperse particle size distribution, and Eq. 5 follows from Goldsmith (1967) for zero slice thickness and $\langle R_v \rangle = m_4/(2m_3)$ where m_3 and m_4 are the 3rd resp. 4th moment of the true particle diameter distribution. The general forms of Eqs. 4 and 5 were derived in detail by Goldsmith (1967). Taking into account the experimental scatter because of a finite number of drops, Eqs. 4 and 5 achieve a sufficient accuracy for our investigations.

To determine the stretch ratio λ_d of the droplets at maximum strain, the samples were quenched and fractured perpendicular and parallel to the loading direction. Assuming that a droplet with an initial radius of r_0 is deformed into an ellipsoidal shape with the principal axes $a = r_0\lambda_d$ and $b = c = r_0\lambda_d^{-1/2}$, estimated values for the stretch ratio λ_d of the droplets at maximum strain ϵ_{max} were obtained using

$$\lambda_d(t' = 0) = \left(\bar{r}/\bar{r}_{perp}\right)^2, \tag{6}$$

where $\bar{r}$ is the average radius of the cross sections of the droplets on the surface of the sample before elongation and $\bar{r}_{perp}$ denotes the average of the radii of the cross sections of the droplets on the surfaces of

the elongated samples which were fractured perpendicular to the loading direction. The estimated $\lambda_d(t' = 0)$ using the number averages follows from $\lambda_{d,n}(t' = 0) = (\langle r_n \rangle / \langle r_{\mathrm{perp},n} \rangle)^2$, and the estimated $\lambda_d(t' = 0)$ using the area averages is given by $\lambda_{d,s}(t' = 0) = (\langle r_s \rangle / \langle r_{\mathrm{perp},s} \rangle)^2$. Here the indices n and s refer to the number average and the area average, respectively. The uncertainty of $\lambda_d(t' = 0)$ calculated by Eq. 6 is at least 10% because the droplets are generally not cut in their center, but at random positions, the stretch ratio depends on the initial radius of each droplet, and the droplet size distribution is not monodisperse.

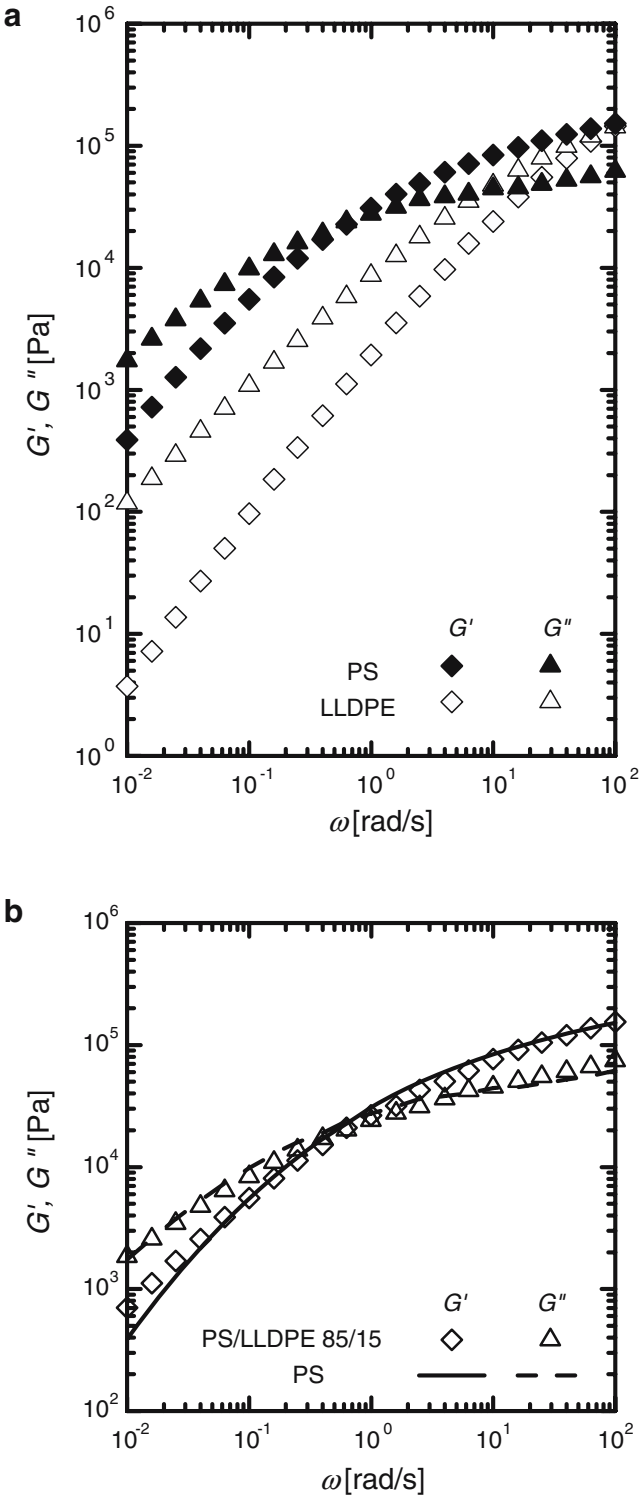

Fig. 1 Storage and loss modulus G' and G'' at $T = 170$ °C as a function of angular frequency ω for (**a**) the blend components and (**b**) pure PS and the PS/LLDPE 85:15 blend

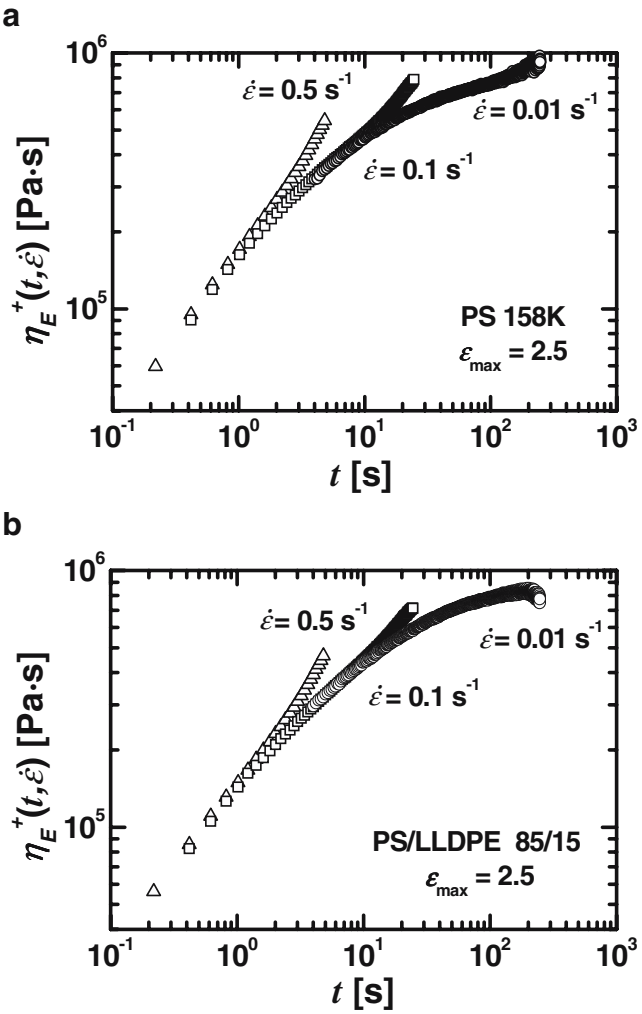

Fig. 2 Transient elongational viscosity $\eta_E^+(t, \dot{\epsilon})$ of (**a**) pure PS and (**b**) the PS/LLDPE 85:15 blend for three different Hencky strain rates $\dot{\epsilon}$ at $T = 170$ °C. The Hencky strain rate is indicated

Results

Figure 1 shows the storage and the loss modulus G' and G'' of the blend components and the PS/LLDPE blend as a function of the angular frequency ω at $T = 170$ °C. The storage and the loss modulus of the PS and the LLDPE attain a shape which is typical of polydisperse polymers, see Fig. 1a. For $\omega < 0.05\,\mathrm{rad\,s^{-1}}$, the storage

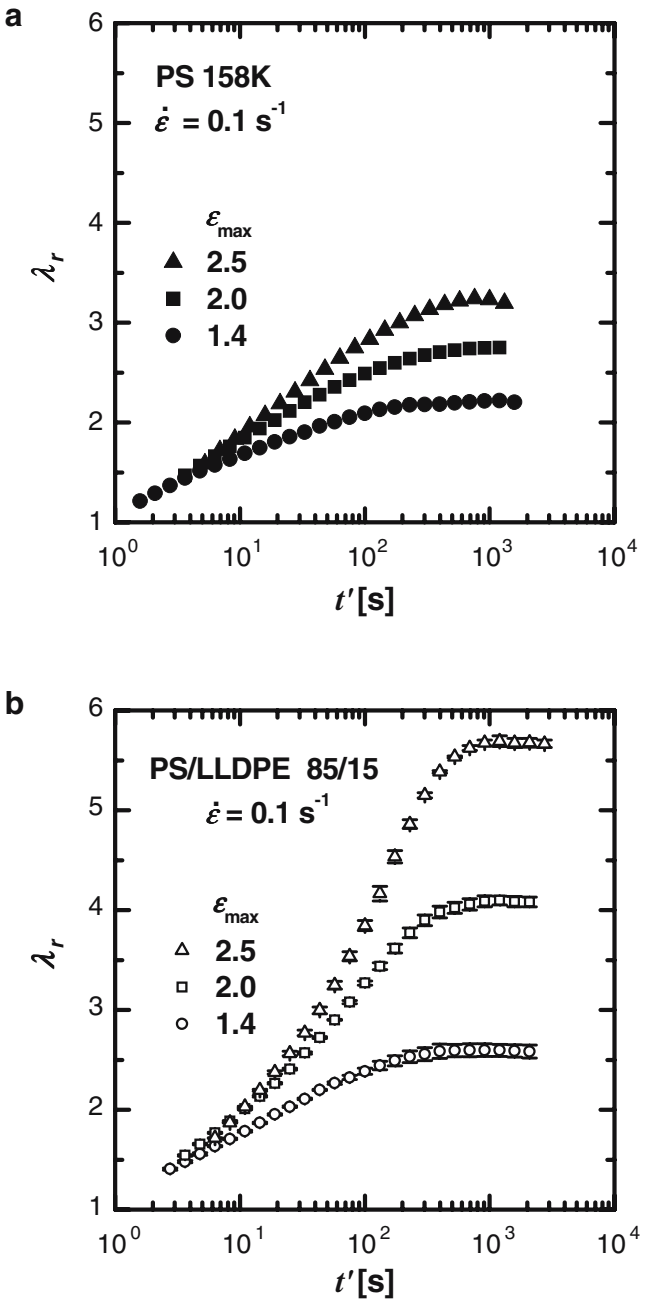

Fig. 3 Dependence of the recovered stretch ratio λ_r on recovery time t' for (**a**) PS and (**b**) the PS/LLDPE 85:15 blend at the elongational rate $\dot{\epsilon} = 0.1$ s^{-1} and the three maximum strains ϵ_{max}. The measurement temperature was $T = 170$ °C

modulus G' of the blend is somewhat larger than G' of the PS (Fig. 1b), although G' of the LLDPE is significantly smaller than G' of the PS. This increase of G' can be interpreted as the onset of a shoulder and is associated with an additional relaxation process caused by the interfacial tension between the two blend components (Palierne 1990; Graebling et al. 1993; Kitade et al. 1997; Okamoto et al. 1999a). Such a behaviour is commonly observed for blends of immiscible polymers. In contrast to G', the loss modulus G'' of the blend only moderately deviates from G'' of the PS, see Fig. 1b.

In Fig. 2, the transient elongational viscosity $\eta_E^+(t, \dot{\epsilon})$ of the PS and the PS/LLDPE blend is presented. The experimental error of $\eta_E^+(t, \dot{\epsilon})$ is about 10%. Whereas the PS and the blend behave linearly viscoelastic for $\dot{\epsilon} = 0.01$ s^{-1}, strain hardening of the PS and the PS/LLDPE blend is observed

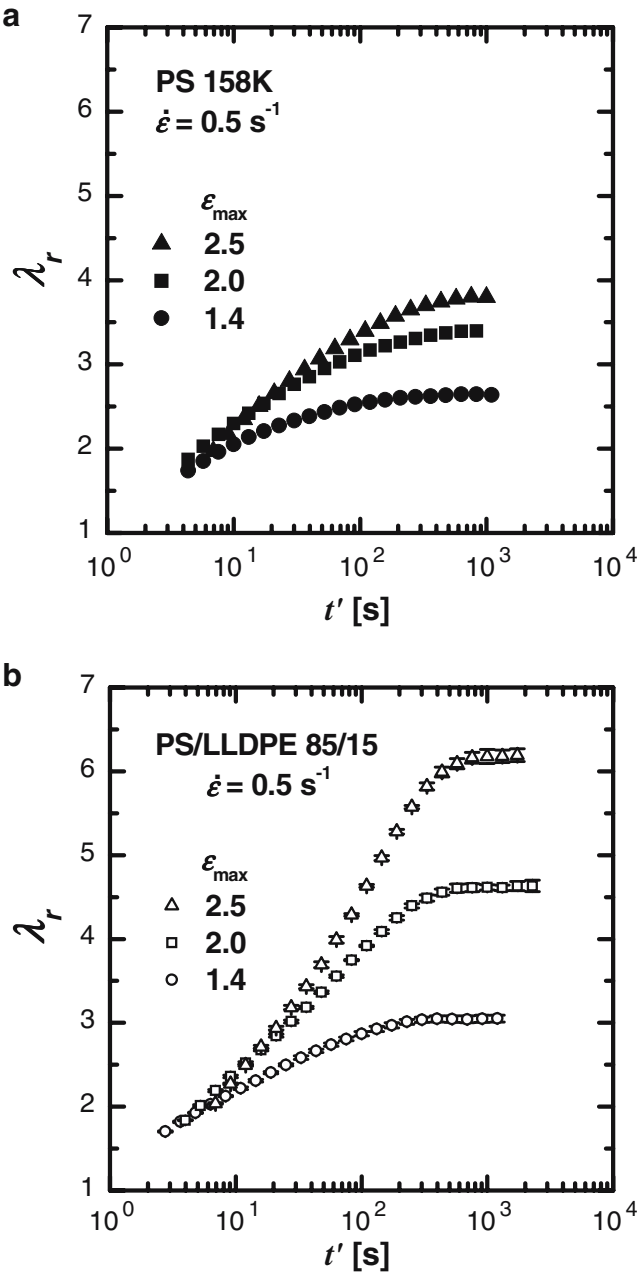

Fig. 4 Dependence of the recovered stretch ratio λ_r on recovery time t' for (**a**) PS and (**b**) the PS/LLDPE 85:15 blend at the elongational rate $\dot{\epsilon} = 0.5$ s^{-1} and the three maximum strains ϵ_{max}. The measurement temperature was $T = 170$ °C

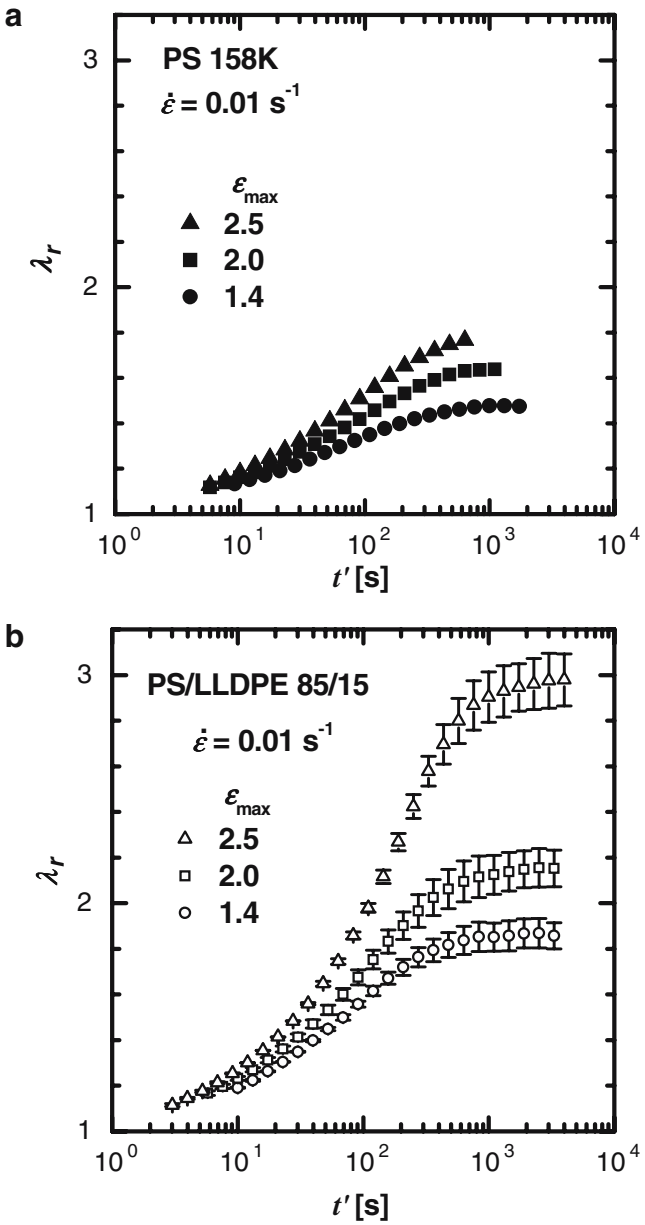

Fig. 5 Dependence of the recovered stretch ratio λ_r on recovery time t' for (**a**) PS and (**b**) the PS/LLDPE 85:15 blend at the elongational rate $\dot{\epsilon} = 0.01\ s^{-1}$ and the three maximum strains ϵ_{max}. The measurement temperature was $T = 170\ ^{o}C$

for $\dot{\epsilon} = 0.1\ s^{-1}$ and $\dot{\epsilon} = 0.5\ s^{-1}$. For the LLDPE strain hardening was not found. The transient elongational viscosity of the PS/LLDPE blend shows less strain hardening than the PS. This reduction of strain-hardening is caused by the low viscous LLDPE droplets in the blend.

Figure 3 presents the transient recovered stretch ratio $\lambda_r(t')$ of the PS and the blend after elongation at $\dot{\epsilon} = 0.1\ s^{-1}$ to various ϵ_{max} values. The relative error of the measurements is less than 5%. The recovered stretch ratio λ_r increases with the recovery time t' and attains a stationary value $\lambda_{r,max}$ at large times for the PS and the blend. The transient recovered stretch ratio $\lambda_r(t')$ and its plateau value $\lambda_{r,max}$ increase with the maximum elongation ϵ_{max} applied. Comparing the data for the PS and the blend shows that λ_r of the blend exceeds the corresponding λ_r of the PS. In Figs. 4 and 5 the transient recovered stretch ratios after elongations at $\dot{\epsilon} = 0.5\ s^{-1}$ and $\dot{\epsilon} = 0.01\ s^{-1}$ are plotted for PS and the blend. The shape of $\lambda_r(t')$ at $\dot{\epsilon} = 0.5\ s^{-1}$ and $\dot{\epsilon} = 0.01\,s^{-1}$ is similar to the shape of $\lambda_r(t')$ at $\dot{\epsilon} = 0.1\ s^{-1}$ (cf. Fig. 3) for PS and the PS/LLDPE 85:15 blend. A more quantitative comparison of the data in Figs. 3 to 5 reveals that $\lambda_r(t')$ increases with elongational rate $\dot{\epsilon}$. In addition, for a constant Hencky strain rate the time t' at which the plateau of $\lambda_r(t')$ starts increases with ϵ_{max} for both PS and the PS/LLDPE 85:15 blend.

Figure 6 shows a typical scanning electron micrograph of the PS/LLDPE blend before elongation. The LLDPE phase forms inclusions which are uniformly dispersed in the PS matrix. The shape of the droplets before elongation is spherical with an average droplet radius $\langle R_n \rangle = 0.87 \pm 0.17\,\mu m$ and $\langle R_v \rangle = 1.12 \pm 0.10\,\mu m$. During melt elongation of the blend, the droplets are stretched. Figure 7a shows a cross section of an elongated sample perpendicular to the loading direction for $\dot{\epsilon} = 0.01\ s^{-1}$ and $\epsilon_{max} = 2.0$. In addition to the cross sections of the individual elongated droplets, the coalescence of two neighboured droplets is shown (see the arrow in Fig. 7a). Table 2 lists the number and the area average of the radii of the cross sections of the droplets and the stretch ratio of the droplets at $\epsilon_{max} = 2.0$. The number and the area average radii $\langle r_{perp,n} \rangle$ and $\langle r_{perp,s} \rangle$ perpendicular to the loading direction are much smaller than the radii $\langle r_n \rangle = 0.68 \pm 0.13\,\mu m$ and $\langle r_s \rangle = 0.99 \pm 0.09\,\mu m$ before

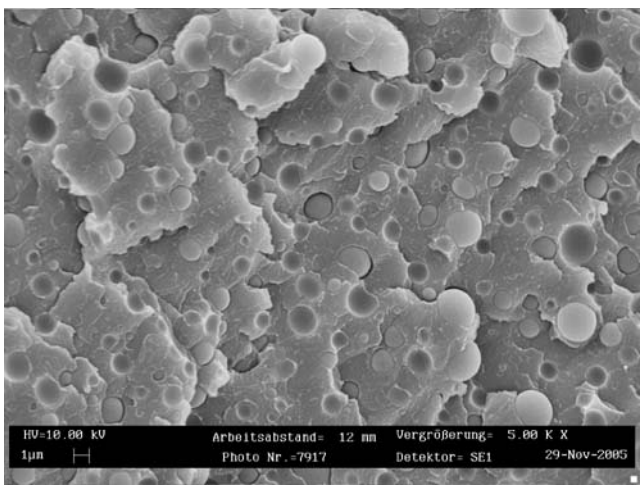

Fig. 6 Scanning electron micrograph of the PS/LLDPE 85:15 blend before elongation

elongation. Figure 7b reveals that spherical ends are formed at the tips of some elongated LLDPE droplets which finally split off the stretched droplets. This phenomenon is called "end-pinching" and leads to the minimization of the interfacial energy. The evolution of the shape of the droplets parallel to the elongation direction during recovery is shown in Fig. 8 for $\dot{\epsilon} = 0.1\ \mathrm{s}^{-1}$ and $\epsilon_{\max} = 2.0$. After $t' = 60$ s of recovery, the droplets attain an ellipsoidal shape with a large stretch ratio, see Fig. 8a. The stretch ratio of the droplets decreases with increasing recovery time t' (cf. Figs. 8b and c), since the interfacial tension causes the recovery of the droplets to their initial spherical shape. At $t' = 480$ s, the droplets have almost attained the spherical geometry, again (Fig. 8d).

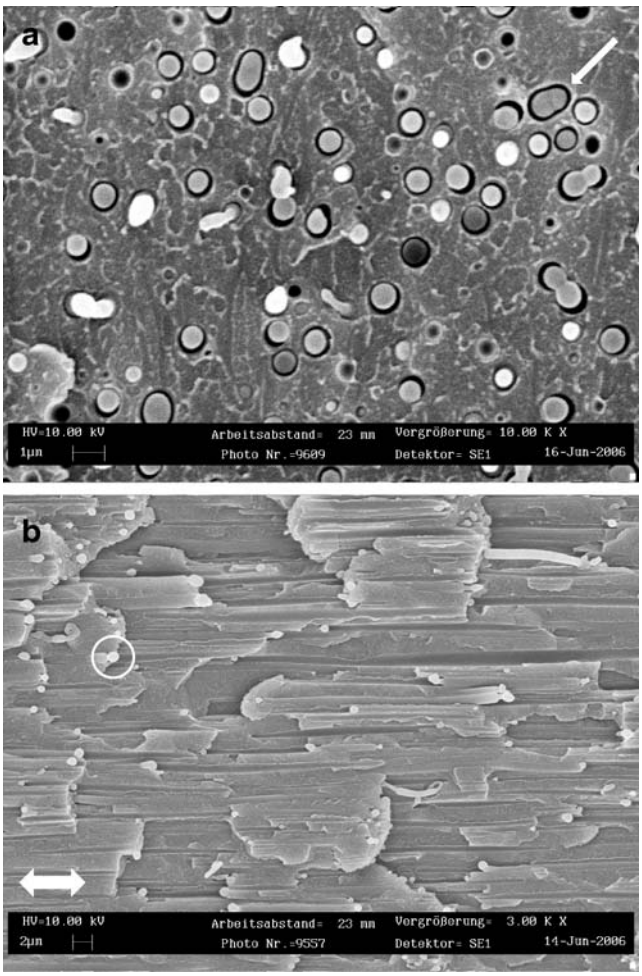

Fig. 7 (**a**) Scanning electron micrograph perpendicular to the loading direction of the PS/LLDPE 85:15 blend at $\epsilon_{\max} = 2.0$ after elongation with $\dot{\epsilon} = 0.01\ \mathrm{s}^{-1}$. (**b**) Scanning electron micrograph parallel to the loading direction of the PS/LLDPE 85:15 blend for $\dot{\epsilon} = 0.1\ \mathrm{s}^{-1}$ and $\epsilon_{\max} = 2.0$ showing the formation of spherical ends at the tips of the elongated droplets ("end-pinching", see the *center of the circle*)

Table 2 The number average $\langle r_{\mathrm{perp},n}\rangle$ and the area average $\langle r_{\mathrm{perp},s}\rangle$ of the radii of the cross-sections perpendicular to the loading direction at maximum strain $\epsilon_{\max} = 2.0$ for the three different Hencky strain rates and the resulting stretch ratio $\lambda_d(t' = 0)$ using Eq. 6

$\dot{\epsilon}$ (s^{-1})	$\langle r_{\mathrm{perp},n}\rangle$ (μm)	$\lambda_{d,n}$	$\langle r_{\mathrm{perp},s}\rangle$ (μm)	$\lambda_{d,s}$
0.01	0.36 ± 0.04	3.6	0.43 ± 0.04	5.3
0.1	0.23 ± 0.02	8.7	0.32 ± 0.03	9.6
0.5	0.26 ± 0.04	6.8	0.32 ± 0.04	9.6

Discussion

Figure 9 presents the maximum recoverable stretch ratio $\lambda_{r,\max}$ as a function of $\lambda_{\max}$ for PS and the blend at the three different Hencky strain rates $\dot{\epsilon}$. The value of $\lambda_{r,\max}$ increases with $\lambda_{\max}$ and $\dot{\epsilon}$ for PS and the blend. The difference between $\lambda_{r,\max}$ of the blend and $\lambda_{r,\max}$ of PS also increases with $\lambda_{\max}$ which indicates that the effect of the recovery of the deformed droplets is more pronounced at higher $\lambda_{\max}$. This trend also agrees with the results of morphological investigations during recovery which show that the stretch ratio of the droplets is larger for $\epsilon_{\max} = 2.5$ than for $\epsilon_{\max} = 2.0$.

The recoverable stretch ratio of the blend is strongly influenced by the recovery of the PS matrix since the molecular recovery of PS is not negligible compared with the recovery of the blend (see Figs. 3 to 5 and Fig. 9). In order to determine the recovery portion which is caused solely by the interfacial tension, the recovery of the PS matrix was subtracted from $\lambda_r(t')$ and $\lambda_{r,\max}$. If the contribution of the interfacial tension to the recovery of the blend is known, the interfacial tension induced recovery portion can be compared then with the effective medium approximation of Handge (2003). This model is based on the assumption that the disperse and the matrix phase are Newtonian fluids and consequently do not contribute to the recoverable stretch by the recovery of the macromolecules.

In this work, a simple additive rule was applied as a first approach. Such a procedure implies the assumption that the molecular recovery of PS is independent of the interfacial tension driven recovery. The recovered stretch which is caused by the interfacial tension is denoted by λ_r^{int} and the experimentally measured recovered stretch of PS by λ_r^{PS}. The additive rule then reads

$$\lambda_r^{\mathrm{int}} = \lambda_r^{\mathrm{blend}} - (1 - \Phi)(\lambda_r^{\mathrm{PS}} - 1), \tag{7}$$

where $\lambda_r^{\mathrm{blend}}$ is the measured recovered stretch of the blend (see Figs. 3 to 5) and Φ the volume fraction of the LLDPE phase. In Eq. 7 the contribution of the molecular recovery of LLDPE to the recovery of the

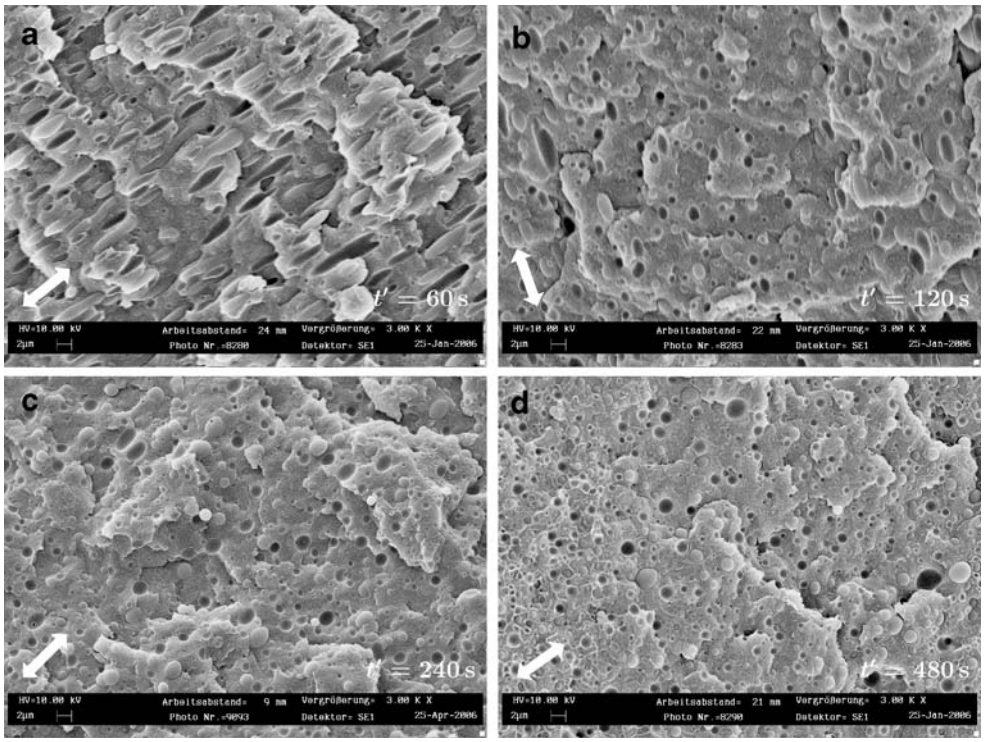

Fig. 8 Scanning electron micrographs of the PS/LLDPE 85:15 blend for $\dot{\epsilon} = 0.1\ s^{-1}$ and $\epsilon_{max} = 2.0$ at the recovery time (**a**) $t' = 60$ s, (**b**) $t' = 120$ s, (**c**) $t' = 240$ s and (**d**) $t' = 480$ s. The *arrows* indicate the direction of elongation

blend is neglected, as it was found to be very small (Heindl 2005). Generally, the rheological properties of a two-phase polymer blend are a nontrivial function of the properties of the blend components and the interface, cf. the linear viscoelastic theory of Palierne (1990) which leads to $\lambda_r(t' \to \infty) = \exp[(\tau_1 - \tau_2)\dot{\epsilon}]$, see the Appendix. However, our analysis of the data revealed that after melt elongation to a large stretch ratio the empirical Eq. 7 is an appropriate approach for the nonlinear regime and also is in agreement with the data of PS/PMMA blends at small t which were studied by Handge and Pötschke (2004).

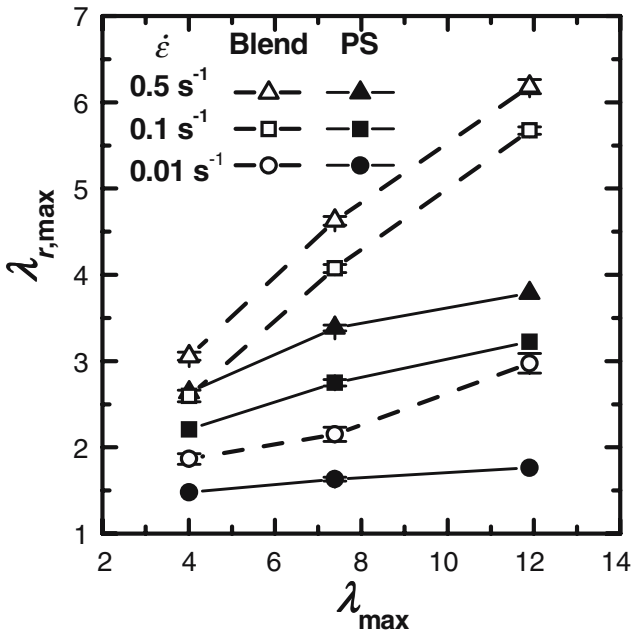

Fig. 9 Maximum recoverable stretch ratio $\lambda_{r,max}$ vs maximum stretch ratio $\lambda_{max} = \exp(\epsilon_{max})$ for the three elongational rates $\dot{\epsilon}$. The temperature was $T = 170$ °C

Using Eq. 7, the experimental values for the interfacial tension induced recovery portion $\lambda_r^{int}(t')$ are determined (see Fig. 10). Similar to the experimental data of the blend, the $\lambda_r^{int}(t')$ values increase with recovery time t' and attain a plateau value $\lambda_{r,max}^{int}$ at long t'. Increasing the maximum elongation leads to increasing $\lambda_r^{int}(t')$ values. Figure 11 presents the dependence of the maximum interfacial tension driven recovery $\lambda_{r,max}^{int}$ on the maximum stretch ratio λ_{max}. The data reveal that $\lambda_{r,max}^{int}$ increases with λ_{max} for the three different Hencky strain rates $\dot{\epsilon}$. The $\lambda_{r,max}^{int}$ value for $\dot{\epsilon} = 0.01\ s^{-1}$ and $\lambda_{max} = 4.0$ does not differ much from the $\lambda_{r,max}^{int}$ values obtained for the two higher strain rates at the same $\lambda_{max} = 4.0$. At higher λ_{max}, the differences become more pronounced, however. The $\lambda_{r,max}^{int}$ values for $\dot{\epsilon} = 0.1\ s^{-1}$ and $\dot{\epsilon} = 0.5\ s^{-1}$ almost superimpose. Consequently, the contribution of the interfacial tension to the total recovery of the blend is similar for $\dot{\epsilon} = 0.1\ s^{-1}$ and $\dot{\epsilon} = 0.5\ s^{-1}$ and is much more pronounced than for $\dot{\epsilon} = 0.01\ s^{-1}$. This result can be explained by

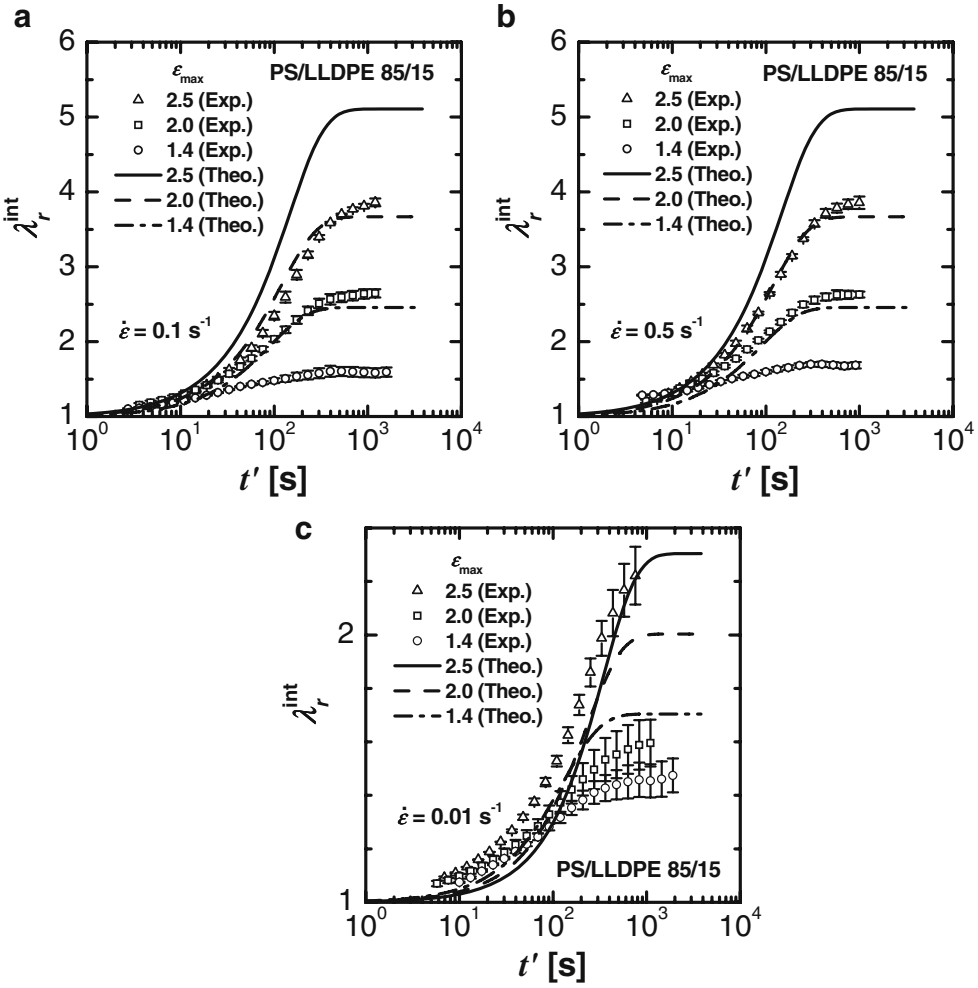

Fig. 10 Experimental (*symbols*) and theoretical (*lines*) transient interfacial tension driven recovery portion λ_r^{int} as a function of recovery time t' for (**a**) $\dot{\epsilon} = 0.1\,s^{-1}$, (**b**) $\dot{\epsilon} = 0.5\,s^{-1}$, and (**c**) $\dot{\epsilon} = 0.01\,s^{-1}$ at $T = 170$ °C. The maximum Hencky strain ϵ_{max} is indicated. The experimental data were calculated using Eq. 7 and the theoretical curves using Eqs. 9 and 10

taking the transient capillary number $Ca_E(t)$ in elongation into account

$$Ca_E(t) = \eta_E^+(t, \dot{\epsilon})\langle R_n\rangle\dot{\epsilon}/(3\Gamma) \tag{8}$$

which is plotted in Fig. 12. The transient capillary number $Ca_E(t)$ is larger than 1 for $\dot{\epsilon} \geq 0.1\,s^{-1}$ and $t \geq 1.5$ s. For small deformations, such large $Ca_E(t)$ values lead to an affine deformation of the droplets during elongation, since for large $Ca_E(t)$ and small deformations the interfacial tension is negligible (Taylor 1934; Delaby et al. 1994, 1995a). On the contrary, for $\dot{\epsilon} = 0.01\ s^{-1}$ the capillary number $Ca_E(t)$ is smaller than 0.6. Hence for $\dot{\epsilon} = 0.01\,s^{-1}$ the droplets are much less deformed than for $\dot{\epsilon} \geq 0.1\,s^{-1}$. For $\dot{\epsilon} = 0.01\,s^{-1}$ the stretch ratio of the droplets strongly depends on $Ca_E(t)$ (Taylor 1934; Delaby et al. 1994, 1995a). Since the interfacial tension induced recovery is related to the extension of the droplets and thus to $Ca_E(t)$, the agreement of the λ_r^{int} values for $\dot{\epsilon} = 0.1\,s^{-1}$ and $\dot{\epsilon} = 0.5\,s^{-1}$ supports the results of Taylor (1934) and Delaby et al. (1994, 1995a) that the stretch ratio of the droplets is independent of $Ca_E(t)$ for $Ca_E(t) \gg 1$. The similarity of the droplet deformation at $\dot{\epsilon} = 0.1\ s^{-1}$ and $\dot{\epsilon} = 0.5\ s^{-1}$ was directly shown by the analysis of the cross sections of the elongated LLDPE particles at the maximum strain $\epsilon_{max} = 2.0$. The number average radii were found as $0.23 \pm 0.02\,\mu m$ for $\dot{\epsilon} = 0.1\,s^{-1}$, $0.26 \pm 0.04\,\mu m$ for $\dot{\epsilon} = 0.5\,s^{-1}$ and $0.36 \pm 0.04\,\mu m$ for $\dot{\epsilon} = 0.01\ s^{-1}$. These data confirm our finding that the $\lambda_{r,max}^{int}$ values of Eq. 7 are equal for $\dot{\epsilon} = 0.1\ s^{-1}$ and $\dot{\epsilon} = 0.5\ s^{-1}$ and support the validity of Eq. 7.

Theoretical description

The determination of the interfacial tension driven recovery portion λ_r^{int} allows to compare the experimental data for the PS/LLDPE blend with the prediction of the effective medium approximation (Handge 2003, 2004a). In this model, two time-evolution equations for the stretch ratio of the sample $\lambda_s = L(t')/L_0$ and the

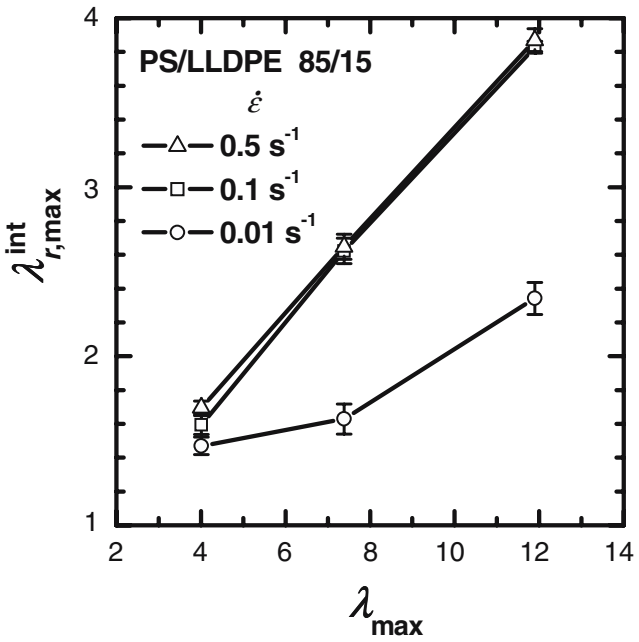

Fig. 11 Maximum interfacial tension-driven recovery portion $\lambda_{r,\max}^{\text{int}}$ (experimental data) as a function of maximum stretch ratio $\lambda_{\max} = \exp(\epsilon_{\max})$ at $T = 170$ °C. The values of $\dot{\epsilon}$ are indicated

droplets $\lambda_d(t')$ were derived where L_0 is the length of the sample before elongation:

$$d\lambda_d/dt' = \left(1 - \lambda_d^{3/2}\right)/[2\tau_m(p + (1-\Phi)\lambda_s/\lambda_d)] \quad (9)$$

$$d\lambda_s/dt' = \left[\Phi + (1-\Phi)\sqrt{\Phi\lambda_s/\lambda_d}\right](\lambda_s/\lambda_d)d\lambda_d/dt'. \quad (10)$$

In Eqs. 9 and 10 $\tau_m = \eta_m r_0/\Gamma$ and $p = \eta_d/\eta_m$ hold, where η_d and η_m denote the zero shear rate viscosities of the droplet phase and the matrix phase, respectively. The volume concentration of the disperse phase is given by Φ. The droplet size distribution before elongation is assumed to be monodisperse with a droplet radius $r_0 = \langle R_n \rangle$ and the droplet shape to be ellipsoidal with the principal axes $a = r_0\lambda_d$ and $b = c = r_0\lambda_d^{-1/2}$ during deformation. At $t' = 0$ we have $\lambda_s(t' = 0) = \lambda_{\max}$. The initial condition for λ_d is given by the true stretch ratio of the droplets at maximum strain $\epsilon_{\max}$. The analytical calculations of Taylor (1934) and Delaby et al. (1994, 1995a) have shown that λ_d depends on the capillary number $\text{Ca}_{\text{Newt}} = \eta_m\dot{\epsilon}r_0/\Gamma$ for Newtonian fluids and consequently on the applied Hencky strain rate $\dot{\epsilon}$. In addition, the volume concentration Φ of the disperse phase also influences the stretch ratio of the droplets. For $\text{Ca}_{\text{Newt}} \ll 1$ we have (see Appendix)

$$\lambda_d(t' = 0) = \exp\{5F(p)\text{Ca}_{\text{Newt}}[1 - \exp(-t_{\max}/\tau_1)]\} \quad (11)$$

and for $\text{Ca}_{\text{Newt}} \gg 1$ (Delaby 1995b)

$$\lambda_d(t' = 0) = 1 + 5(\lambda_{\max} - 1)/[2p + 3 - 2\Phi(p-1)] \quad (12)$$

with $F(p) = (19p + 16)/[40(p+1) - 8\Phi(5p+2)]$, $\tau_1 = \eta_m r_0\,[2p + 3 - 2\Phi\,(p-1)]\,(19p+16)/\{4\Gamma[10(p+1) - 2\Phi\,(5p+2)]\}$ and $t_{\max} = \epsilon_{\max}/\dot{\epsilon}$.

Using a Runge-Kutta scheme, the time-evolution equations 9 and 10 were numerically solved for the parameters $\Phi = 0.17$, $p = 0.059$, $r_0 = 0.9\,\mu$m, $\Gamma = 5\,\text{mNm}^{-1}$, $\eta_m = 2.3 \cdot 10^5$ Pas and $\tau_m = 41.4$ s of the PS/LLDPE blend. The elongation experiments with $\dot{\epsilon} = 0.01$ s^{-1} correspond to $\text{Ca}_{\text{Newt}} < 1$ and the elongation experiments with $\dot{\epsilon} = 0.1$ s^{-1} and $\dot{\epsilon} = 0.5$ s^{-1} to $\text{Ca}_{\text{Newt}} \gg 1$. The theoretical prediction of the interfacial tension driven recovery portion follows from $\lambda_r^{\text{int}}(t') = L_{\max}/L(t') = \lambda_{\max}/\lambda_s(t')$.

In Fig. 10, the theoretical results for $\lambda_r^{\text{int}}(t')$ are plotted and compared with the experimental data based on Eq. 7. The numerical solution for λ_r^{int} equals one for $t' = 0$ and increases with recovery time t' until it attains a stationary value $\lambda_{r,\max}^{\text{int}}$. Figure 10 reveals that the time scale of recovery based on the numerical solution agrees well with the time scale of the experimental data. The stationary value of the interfacial tension driven recovery portion increases with the maximum Hencky strain $\epsilon_{\max}$, both for the model prediction and the experimental data. In addition, the results of the effective medium approximation show an increase with elongational rate $\dot{\epsilon}$ similar to the experimental λ_r^{int} data. However, the absolute values of the solutions of Eqs. 9 and 10 exceed the corresponding experimental $\lambda_r^{\text{int}}(t')$ values for $\dot{\epsilon} = 0.1$ s^{-1} and $\dot{\epsilon} = 0.5$ s^{-1}. For $\dot{\epsilon} = 0.1$ s^{-1} and $\dot{\epsilon} = 0.5$ s^{-1} the deviations between theory and experiment can be explained by various effects which

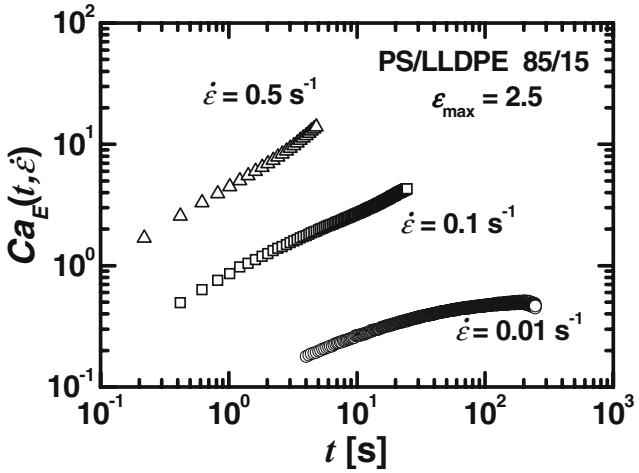

Fig. 12 Transient capillary number $\text{Ca}_E(t)$ in elongation of the PS/LLDPE 85:15 blend for the three different Hencky strain rates $\dot{\epsilon}$, see Eq. 8

all indicate that the true λ_r^{int} values are larger than the λ_r^{int} values obtained by Eq. 7. First, the investigation of the morphology at maximum strain ϵ_{max} (cf. Fig. 7a) revealed that λ_d derived from Eq. 12 is larger than the true stretch ratio λ_d at $t' = 0$. For example, we find $\lambda_{d,exp}/\lambda_{d,Eq.12} \approx 8.7/10.3 = 0.84$ for $\dot{\epsilon} = 0.1\,s^{-1}$ and $\epsilon_{max} = 2.0$. Secondly, in contrast to the PS/PMMA blends investigated by Gramespacher and Meissner (1997) and Handge and Pötschke (2004) end-pinching was observed for the PS/LLDPE blend, see Fig. 7b. The end-pinching phenomenon is not taken into account by the effective medium approximation, but influences the time-dependent recovery. By end-pinching, a droplet decreases the interfacial energy and the stretch ratio of the droplet in such a way that it does not contribute significantly to the total recovery of the blend. In addition, the term $(1 - \Phi)\lambda_r^{PS}$ in Eq. 7 may overestimate the contribution of the PS phase to the total recovery of the blend, since shear deformation may occur in the PS phase around the LLDPE particles (Delaby et al. 1994, 1995a). Finally, because of $p \ll 1$ the PS phase in the blend is elongated with an average strain rate which is smaller than the macroscopic strain rate $\dot{\epsilon}$ for $\dot{\epsilon} \geq 0.1\ s^{-1}$. This reduction of the average strain rate of the PS phase also leads to a molecular recovery of the PS molecules which is smaller in the blend than measured for PS alone; i.e., the recoverable portion taken into account by the additive rule Eq. 7 is too high.

Conclusions

The dependence of the recovered stretch ratio λ_r on the recovery time t' at various elongational rates and maximum elongations was investigated for PS and a 85 wt.% PS/15 wt.% LLDPE blend at $T = 170\ ^{o}C$. The recovered stretch ratio of the PS and the blend increases with recovery time and attains a stationary value at large recovery times. In addition, $\lambda_r(t')$ increases with elongational rate $\dot{\epsilon}$ and maximum elongation ϵ_{max} for the PS and the blend. The comparison of the transient recovery of the blend and of the PS showed that the recovered stretch of the blend strongly exceeds the corresponding $\lambda_r(t')$ value of the PS. The investigation of the morphology during recovery revealed that the difference between the recovered stretch ratios of the blend and of the PS results from the recovery of elongated droplets driven by the interfacial tension between PS and LLDPE. In addition to the retraction of elongated LLDPE droplets to spheres, the formation of small spherical ends at the tips of the elongated droplets (the so-called end-pinching phenomenon) was observed during recovery. A simple additive rule expressed by Eq. 7 was used to extract the interfacial tension driven recovery portion $\lambda_r^{int}(t')$ from the total recovery $\lambda_r^{blend}(t')$ of the blend. The experimental data for $\lambda_r^{int}(t')$ were compared with the results of the effective medium approximation of Handge (2003). The model reproduces the basic trends of the experimental data for various sets of elongational rates and maximum elongations, namely the time scale of recovery and the increase of λ_r^{int} with $\dot{\epsilon}$ and ϵ_{max}. The reasons for the deviations of the absolute values determined by the model and the experiments can be sought in the unknown true stretch ratios of the droplets at maximum elongation, the break-up of elongated droplets by end-pinching and the unknown exact contribution of the molecular recovery of the PS phase.

Acknowledgements Parts of this work were financially supported by the German Research Foundation (DFG). Scanning electron micrographs were made by Dipl.-Ing. M. Papp. A program to calculate recovery data was developed by Dipl.-Ing. S. Schuberth using MATLAB. The discussions with Dipl.-Ing. N. Katsikis, Dipl.-Ing. A. Kirchberger, Dr. A. KHassanova and Dr. M. Heindl are gratefully acknowledged. Dr. M. Heindl also supplied the blend.

Appendix Stretch ratio of droplets for small Ca_{Newt}

Stretch ratio of droplets for small Ca_{Newt}

Graebling et al. (1993) have shown that the model of Palierne (1990) for a nondilute emulsion of two Newtonian fluids with equally sized droplets of radius r_0 can be modelled by a Jeffreys model which consists of a Maxwell element (spring constant G_1 and dashpot viscosity η_1) in parallel with a dashpot of viscosity η_2. The following relations hold between the blend parameters $\Phi, r_0, \Gamma, \eta_m$ and $p = \eta_d/\eta_m$ and the parameters G_1, $\tau_1 = \eta_1/G_1$ and $\tau_2 = \eta_1\eta_2/[(\eta_1 + \eta_2)G_1]$ of the Jeffreys model (Graebling et al. 1993):

$$G_1 = 20\Phi\Gamma/\{r_0[2p + 3 - 2\Phi(p - 1)]^2\} \quad (13)$$

$$\tau_1 = \eta_m r_0[2p + 3 - 2\Phi(p - 1)](19p + 16) / \{4\Gamma[10(p + 1) - 2\Phi(5p + 2)]\} \quad (14)$$

$$\tau_2 = \eta_m r_0[2p + 3 + 3\Phi(p - 1)](19p + 16) / \{4\Gamma[10(p + 1) + 3\Phi(5p + 2)]\}. \quad (15)$$

If $x_1(t)$ denotes the elongation of the spring with elastic constant G_1, $\tilde{x}_1(t)$ the elongation of the dashhpot with viscosity η_1 and $x_0(t) = x_1(t) + \tilde{x}_1(t)$ the total elongation of the Jeffreys model, then the transient elongation

of the spring during a startup flow at a constant elongational rate $\dot{x}_0 = \text{constant}$ for $t \geq 0$ is

$$x_1(t) = \dot{x}_0 \tau_1 \left[1 - \exp\left(-t/\tau_1\right)\right]. \quad (16)$$

Comparing the surface energy of a stretched droplet with the elastic energy of the spring, see Delaby (1995b), one finds for the Hencky strain of a droplet $\epsilon_d = \ln \lambda_d = 5x_1/[2p + 3 - 2\Phi(p-1)]$. Then Eq. 16 leads to the stretch ratio of the droplets in a nondilute emulsion at a low capillary number $\text{Ca}_{\text{Newt}} = \eta_m \dot{\epsilon} r_0 / \Gamma$ by inserting the expression for τ_1 and replacing $\dot{x}_0$ by $\dot{\epsilon}$ into Eq. 16:

$$\lambda_d(t' = 0) = \exp\{5F(p)\text{Ca}_{\text{Newt}}[1 - \exp\left(-t/\tau_1\right)]\}, \quad (17)$$

with $F(p) = (19p + 16)/[40(p+1) - 8\Phi(5p+2)]$. Finally, the equilibrium shear compliance J_e^0 of the Jeffreys model can be also calculated (Vinckier et al. 1999) and is given by $J_e^0 = (\tau_1 - \tau_2)/(\eta_1 + \eta_2)$. This leads to the recoverable elongational Hencky strain $\epsilon_r(t' \to \infty) = J_e^0(\eta_1 + \eta_2)\dot{\epsilon} = (\tau_1 - \tau_2)\dot{\epsilon}$ in the linear viscoelastic regime (Laun and Münstedt 1978).

References

Almusallam AS, Larson RG, Solomon MJ (2000) A constitutive model for the prediction of ellipsoidal droplet shapes and stresses in immiscible blends. J Rheol 44(5):1055–1083

Delaby I, Ernst B, Germain Y et al (1994) Droplet deformation in polymer blends during uniaxial elongational flow: Influence of viscosity ratio for large capillary numbers. J Rheol 38(6):1705–1720

Delaby I, Ernst B, Muller R (1995a) Drop deformation during elongational flow in blends of viscoelastic fluids. Small deformation theory and comparison with experimental results. Rheol Acta 34(6):525–533

Delaby I (1995b) Deformation transitoire d'inclusions dans des mélanges de polymères incompatibles en écoulement elongationnel uniaxial. PhD dissertation, University of Strasbourg. pp 44–46

Doi M, Ohta T (1991) Dynamics and rheology of complex interfaces. I. J Chem Phys 95(2):1242–1248

Fahrländer M, Friedrich C (1999) Rheological properties of polymer blends with sphere-in-sphere morphology. Rheol Acta 38(3):206–213

Filipe S, Cidade MT, Maia JM (2006) Uniaxial extensional flow behavior of immiscible and compatibilized polypropylene/liquid crystalline polymer blends. Rheol Acta 45(3): 281–289

Goldsmith PL (1967) The calculation of true particle size distributions from the sizes observed in a thin slice. Br J Appl Phys 18:813–830

Graebling D, Muller R, Palierne JF (1993) Linear viscoelastic behavior of some incompatible polymer blends in the melt. Interpretation of data with a model of emulsion of viscoelastic liquids. Macromolecules 26(2):320–329

Gramespacher H, Meissner J (1995) Reversal of recovery direction during creep recovery of polymer blends. J Rheol 39(1):151–160

Gramespacher H, Meissner J (1997) Melt elongation and recovery of polymer blends, morphology, and influence of interfacial tension. J Rheol 41(1):27–44

Gronski W, Läuger J, Laubner C (1996) Structure development under shear flow during spinodal decomposition of a polymer blend observed by simultaneous measurement of small angle light scattering and rheological functions. J Mol Struct 383:23–30

Handge UA (2003) Modeling recovery of polymer blends after melt elongation. J Rheol 47(4):969–978

Handge UA (2004) Recovery of polymer blends after melt elongation: analysis of a model for small and large capillary numbers, third international symposium on slow dynamics in complex systems, November 3-8, 2003. Sendai. AIP Conf Proc 708:52–55

Handge UA, Pötschke P (2004) Interplay of rheology and morphology in melt elongation and subsequent recovery of polystyrene/poly(methyl methacrylate) blends. J Rheol 48(5):1103–1122 [Erratum 49(6):1553, 2005]

Handge UA (2005) Experimental investigation of equibiaxial extension and breakup of drops in a molten two-phase polymer blend. Phys Rev E 72:011801-1-011801-5

Heindl M, Sommer MK, Münstedt H (2004) Morphology development in polystyrene/polyethylene blends during uniaxial elongational flow. Rheol Acta 44(1):55–70

Heindl M (2005) Einfluss von Dehnströmungen auf die Morphologieausbildung in Polymerblends. PhD dissertation, University Erlangen-Nürnberg. Shaker, Aachen

Iza M, Bousmina M (2000) Nonlinear rheology of immiscible polymer blends: step strain experiments. J Rheol 44(6):1363–1384

Jacobs U, Fahrländer M, Winterhalter J, Friedrich C (1999) Analysis of Palierne's emulsion model in the case of viscoelastic interfacial properties. J Rheol 43(6):1495–1509

Kitade S, Ichikawa A, Imura N et al (1997) Rheological properties and domain structures of immiscible polymer blends under steady and oscillatory shear flows. J Rheol 41(5):1039–1060

Laun HM, Münstedt H (1978) Elongational behaviour of a low density polyethylene melt. I. Strain rate and stress dependence of viscosity and recoverable strain in the steady-state. Comparison with shear data. Influence of interfacial tension. Rheol Acta 17(4):415–425

Levitt L, Macosko CW, Schweizer T et al (1997) Extensional rheometry of polymer multilayers: a sensitive probe of interfaces. J Rheol 41(3):671–685

Mechbal N, Bousmina M (2004) Uniaxial deformation and relaxation of polymer blends: relationship between flow and morphology development. Rheol Acta 43(2):119–126

Minale M, Moldenaers P, Mewis J (1997) Effect of shear history on the morphology of immiscible polymer blends. Macromolecules 30(18):5470–5475

Münstedt H (1979) New universal extensional rheometer for polymer melts. Measurements on a polystyrene sample. J Rheol 23(4):421–436

Münstedt H, Kurzbeck S, Egersdörfer L (1998) Influence of molecular structure on rheological properties of polyethylenes: Part II. Elongational behavior. Rheol Acta 37(1):21–29

Okamoto K, Takahashi M, Yamane H et al (1997) Droplet phase and dynamic viscoelasticity of PMMA/PS blend melts. Nihon Reoroji Gakkaishi 25(4):199–200

Okamoto K, Takahashi M, Yamane H, Kashihara H, Masuda T (1999a) Shape recovery of a dispersed droplet phase and stress relaxation after application of step shear strains in a

polystyrene/polycarbonate blend melt. J Rheol 43(4):951–965

Okamoto K, Takahashi M, Yamane H et al (1999b) Measurement of interfacial tension between polymer melts: improved imbedded fiber retraction, breaking thread and dynamic viscoelasticity methods. Nihon Reoroji Gakkaishi 27(2):109–115

Oosterlink F, Mours M, Laun HM et al (2005) Morphology development of a polystyrene/polymethylmethacrylate blend during start-up of uniaxial elongational flow. J Rheol 49(4): 897–918

Palierne JF (1990) Linear rheology of viscoelastic emulsions with interfacial tension. Rheol Acta 29(3):204–214 [Erratum 30(5):497, 1991]

Takahashi Y, Kurashima N, Noda I et al (1994a) Experimental tests of the scaling relation for textured materials in mixtures of two immiscible fluids. J Rheol 38(3):699–712

Takahashi Y, Kitade S, Kurashima N, Noda I (1994b) Viscoelastic properties of immiscible polymer blneds under steady and transient shear flows. Polym J (Tokyo) 26(11): 1206–1212

Takahashi Y, Noda I (1995) Immiscible polymer blends under shear flow. In: Nakatani AI, Dadmun MD (eds) Flow induced structure in polymers. American Chemical Society, Washington, DC, 140–152

Taylor GI (1934) The formation of emulsions in definable fields of flow. Proc R Soc Lond Ser A 146:501–523

Thornton BA, Villasenor RG, Maxwell B (1980) The melt elasticity of polymer blends: polystyrene/poly(methyl methacrylate). J Appl Polym Sci 25(4):653–663

Vinckier I, Moldenaers P, Mewis J (1996) Relationship between rheology and morphology of model blends in steady shear flow. J Rheol 40(4):613–631

Vinckier I, Moldenaers P, Mewis J (1997) Transient rheological response and morphology evolution of immiscble polymer blends. J Rheol 41(3):705–718

Vinckier I, Moldenaers P, Mewis J (1999) Elastic recovery of immiscible blends. 1. Analysis after steady state shear flow. Rheol Acta 38(1):65–72

Wagner NJ, Öttinger HC, Edwards BJ (1999) Generalized Doi-Ohta model for multiphase flow developed via Generic. AIChE J 45(6):1169–1181

Wetzel ED, Tucker CL (2001) Droplet deformation in dispersions with unequal viscosities and zero interfacial tension. J Fluid Mech 426:199–228

Wu S (1982) Polymer interface and adhesion. Dekker, New York